Controlling reflections from mesh refinement interfaces in numerical relativity

John G. Baker[1] and James R. van Meter[1]

[1]*Laboratory for Gravitational Astrophysics, NASA Goddard Space Flight Center, Greenbelt, Maryland 20771*

A leading approach to improving the accuracy on numerical relativity simulations of black hole systems is through fixed or adaptive mesh refinement techniques. We describe a generic numerical error which manifests as slowly converging, artificial reflections from refinement boundaries in a broad class of mesh-refinement implementations, potentially limiting the effectiveness of mesh-refinement techniques for some numerical relativity applications. We elucidate this numerical effect by presenting a model problem which exhibits the phenomenon, but which is simple enough that its numerical error can be understood analytically. Our analysis shows that the effect is caused by variations in finite differencing error generated across low and high resolution regions, and that its slow convergence is caused by the presence of dramatic speed differences among propagation modes typical of 3+1 relativity. Lastly, we resolve the problem, presenting a class of finite-differencing stencil modifications which eliminate this pathology in both our model problem and in numerical relativity examples.

PACS numbers: put pacs numbers here

I. INTRODUCTION

Recent years have seen a dramatic rise in opportunities for observing strong-field gravitational dynamics. New observations of dense black-hole-like objects, both at stellar, and supermassive scales are increasingly frequent. Anticipated gravitational wave observations by ground-based and space-based detectors are expected to capture information about these objects at moments of the strongest gravitational interactions. Interpretation of data from any such observations will depend on theoretical modeling of the strong-field interactions of dense black-hole-like objects in the process of generating gravitational radiation. General Relativity is the standard model for describing gravitational interactions and wave generation. Unfortunately, the predictions of General Relativity for such cases are not yet fully understood, but will depend on 3-D numerical relativity computer simulations.

While numerical relativity has progressed markedly in recent years, significant improvements in the fidelity of models for events such as binary black hole coalescence will be essential for the full interpretation of upcoming observations. There are many facets to the problem of improving such simulation, including optimally formulating of Einstein's equations, properly handling boundaries, handling black hole singularities, handling constraint violations, and making judicious gauge choices. There are also basic numerical issues concerning how to, with finite resources, perform such high-fidelity 3-D simualtions with strong short wavelength gravitational features near the sources, and weak but critical long-wavelength gravitational (radiation) features emerging in a large domain. Approaches to this latter class of issues include, developing higher-order accurate finite differencing methods, spectral methods, mesh-refinement techniques and other forms of numerical patching techniques.

We focus here on resolving a limitation which has arisen in our work on mesh refinement techniques, but which may have analogues in other numerical patching treatments as well. Mesh refinement techniques divide the computational domain into regions with separate computational grids which can be of higher resolution in some regions than others. Such approaches invlove mesh-structure interfaces across which the details of the finite-differencing treatment suddently change. Inevitably, these interfaces contribute to computational error, manifesting such effect as "reflections" off the interfaces. Considerable attention is given to implementing "clean" interfaces, which generate small error, compared to error generated in the bulk regions. At minimum, this requires interface induced error to converge at least as rapidly as the bulk error. For some classes of black hole evolutions, with non-vanishing shift advection terms, we have typically observed large error propagating from mesh interfaces. This problem forms the focus of this paper.

II. INTERFACE PERFORMANCE

The pertinent features of our numerical scheme are as follows. We are solving the 3+1 BSSN formulation of Einstein's equations. Our gauge condition is numerically determined, typically with some variation of the 1+log slicing and hyperbolic Gamma-driver shift evolution equations. All spatial derivatives are computed by 2nd order accurate, centered differencing, save for advection derivatives, for which we use 2nd order accurate upwinded differencing.

To resolve any sources, such as black holes, adequately, whilst pushing the computational grid boundary sufficiently far away, we use fixed mesh refinement (FMR), as implemented by a software package for this purpose called Paramesh. With this implementation, the resolutions of two adjacent refinement regions always differ by a factor of two; i.e. the grid-spacing of the coarser region is double what it is in the finer region. "Ghostzones" or

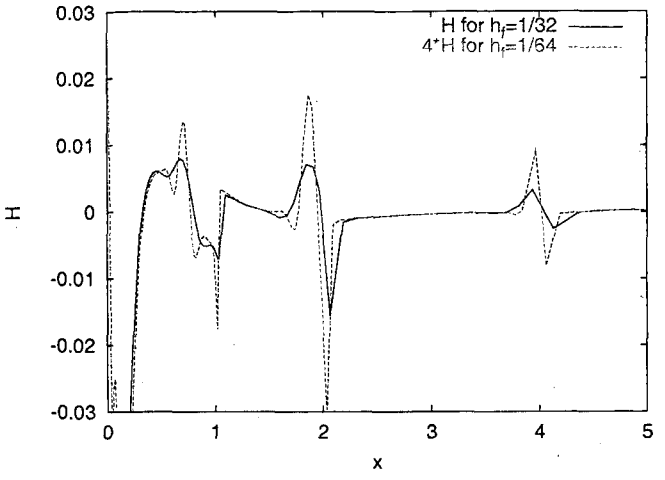

FIG. 1: Convergence plot for the Hamiltonian constraint H at time $t = 4M$. There is a single puncture black hole centered at the origin, and refinement boundaries at $|x_i| = 1M$, $2M$, and $4M$. The finest grid spacing h_f for each simulation is indicated in the figure, and the higher resolution is multiplied by a factor of 4, as appropriate for demonstrating 2nd order convergence.

"guardcells", typically two layers, are required to provide buffering between refinement levels. These guardcells are filled in by interpolation.

Whether the simulation performs adequately in the presence of refinement interfaces is a question of particular concern to us. Of course, refinement boundaries are sources for reflection, but these reflections are, generally speaking, satisfactorally convergent and often negligible. An exception has plagued us in the case of a non-negligible shift across a refinement boundary. In this case, we observe reflection that propagates at a velocity of $-\beta^i$, that is not clearly converging at an appropriate rate, and that, in some situations, dominates the error. This pathology is most evident in the Hamiltonian constraint as computed from the evolution of a single Brill-Lindquist puncture black hole (Fig. 1).

III. A MODEL PROBLEM

A. Linearized BSSN system

To understand the source of the β-speed error exhibited in the last section, we begin by considering a linearized BSSN system with 1+log slicing and hyperbolic Gamma-driver shift. The system of equations is:

$$\dot{a} = -2K \tag{1}$$

$$\dot{B}^i = \dot{\tilde{\Gamma}}^i \tag{2}$$

$$\dot{\beta}_1^i = \frac{3}{4}B \tag{3}$$

$$\dot{\phi} = -\frac{1}{6}(K - \partial_i\beta_1^i) + \beta_0^k\partial_k\phi \tag{4}$$

$$\dot{K} = -\partial_i\partial_i a + \beta_0^k\partial_k K \tag{5}$$

$$\dot{h}_{ij} = -2\tilde{A}_{ij} + \partial_i\beta_1^j + \partial_j\beta_1^i - \frac{2}{3}\delta_{ij}\partial_k\beta_1^k + \beta_0^k\partial_k h_{ij} \tag{6}$$

$$\dot{\tilde{A}}_{ij} = \Big[-\partial_i\partial_j a - \frac{1}{2}\partial_k\partial_k h_{ij} + \frac{1}{2}\partial_i\tilde{\Gamma}^j + \frac{1}{2}\partial_j\tilde{\Gamma}^i - 2\partial_i\partial_j\phi\Big]^{\rm TF} + \beta_0^k\partial_k\tilde{A}_{ij} \tag{7}$$

$$\dot{\tilde{\Gamma}}^i = -\frac{4}{3}\partial_i K + \partial_k\partial_k\beta_1^i + \frac{1}{3}\partial_i\partial_j\beta_1^j + \beta_0^k\partial_k\tilde{\Gamma}^i \tag{8}$$

where $a \equiv \alpha - 1$, $\beta_1^i \equiv \beta^i - \beta_0^i$, (with β_0^i assumed spatially uniform for simplicity), and $h_{ij} \equiv \tilde{\gamma}_{ij} - \delta_{ij}$.

For a one-dimensional problem, if we assume plane-wave solutions (generalizable by Fourier analysis), then the above system of equations can be written in the form:

$$\partial_t|u\rangle = ik\mathsf{M}|u\rangle \tag{9}$$

where

$$|u\rangle = \begin{pmatrix} \hat{a} \\ \hat{B} \\ \hat{\beta}_1 \\ \hat{\phi} \\ \hat{K} \\ \hat{h} \\ \hat{A} \\ \hat{\Gamma} \end{pmatrix} e^{i(kx-\omega t)} \tag{10}$$

and

$$\mathsf{M} = \begin{pmatrix} 0 & 0 & 0 & 0 & \frac{2}{ik} & 0 & 0 & 0 \\ 0 & 0 & \frac{4ik}{3} & 0 & \frac{4}{3} & 0 & 0 & -\beta_0 \\ 0 & \frac{3}{4ik} & 0 & 0 & 0 & 0 & 0 & 0 \\ 0 & 0 & -\frac{1}{6} & -\beta_0 & -\frac{1}{6ik} & 0 & 0 & 0 \\ -ik & 0 & 0 & 0 & -\beta_0 & 0 & 0 & 0 \\ 0 & 0 & -\frac{4}{3} & 0 & 0 & -\beta_0 & -\frac{2}{ik} & 0 \\ -\frac{2ik}{3} & 0 & 0 & -\frac{4ik}{3} & 0 & -\frac{ik}{2} & -\beta_0 & -\frac{2}{3} \\ 0 & 0 & \frac{4ik}{3} & 0 & \frac{4}{3} & 0 & 0 & -\beta_0 \end{pmatrix} \tag{11}$$

The eigenvalues are $0, -\beta_0, -\beta_0+1, -\beta_0-1, -\frac{1}{2}\beta_0 + \frac{1}{2}\sqrt{\beta_0^2+8}, -\frac{1}{2}\beta_0 - \frac{1}{2}\sqrt{\beta_0^2+8}, -\frac{1}{2}\beta_0 + \frac{1}{2}\sqrt{\beta_0^2+4}$, and $-\frac{1}{2}\beta_0 - \frac{1}{2}\sqrt{\beta_0^2+4}$.

If $|\lambda\rangle$ is the eigenvector associated with eigenvalue λ, and $\langle\lambda|$ is defined such that $\sum_\lambda |\lambda\rangle\langle\lambda| = \mathsf{I}$, then

$$\mathsf{M} = \sum_\lambda \lambda|\lambda\rangle\langle\lambda| \tag{12}$$

By substituting Eq. (12) into Eq. (9) the system of evolution equations can be decomposed into a series of advection terms, each associated with a characteristic velocity equal to one of the eigenvalues. Note that, assuming $\beta_0 \ll 1$, the β-speed mode is much slower than any of the other non-zero-speed modes. As we are particularly concerned with this mode, it is instructive to write the evolution equation thusly:

$$\partial_t \begin{pmatrix} a \\ B \\ \beta_1 \\ \phi \\ K \\ h \\ A \\ \Gamma \end{pmatrix} = -\beta_0 \partial_x \begin{pmatrix} 0 \\ 0 \\ 0 \\ -\frac{3}{8} \\ 0 \\ 1 \\ 0 \\ 0 \end{pmatrix} \left(-\frac{8}{3}\phi - \frac{1}{3ik}\Gamma \right) + \sum_{\lambda \neq -\beta_0} \lambda \partial_x |\lambda\rangle\langle\lambda|u\rangle \qquad (13)$$

This equation indicates that disturbances originating in ϕ and Γ can propagate in ϕ and h at β-speed and further, that this is the only means of β-speed propagation allowed by this system. Thus ϕ is uniquely significant in both generating and propagating β-speed modes.

B. "Bumpy" system

Less formally it is clear that Eq. (13) resembles the $\dot{\phi}$ evolution equation in the BSSN system. The simplest model for the generation and propagation of the β-speed modes would be one dimensional advection equation with an additional driving term,

$$\frac{\partial \varphi}{\partial t}(x,t) = \beta \frac{\partial \varphi}{\partial x}(x,t) + f(x,t), \qquad (14)$$

In our numerical simulations, it appears that the reflected 'bumps' may be triggered by a rapidly propagating gauge pulse which propagates outward early in the simulations. For our model problem, which we will term "Bumpy" because of its most salient feature, we will drive the advection equation with a pulse propagating at speed v, significantly faster than the advection speed β. We thus let $f(x,t) = f(x - vt)$ where v is larger than β and both are assumed positive. This model equation is simple enough to be solved directly,

$$\begin{aligned} \varphi(x,t) &= \int_0^t f(x + (t-t')\beta, t')\mathrm{d}t' \\ &= \frac{-1}{v+\beta}(F(x-vt) - F(x+\beta t)). \end{aligned} \qquad (15)$$

For definiteness we can take the driving term to be a Gaussian pulse, $f(x) = \exp(-x^2)$, implying $F(x) = (\sqrt{(\pi)}/2)\mathrm{erf}(x)$. For a localized pulse, such as this, the $F(x+\beta t)$ term in the exact solution will be negligible in the region of interest, near $x = x_0$.

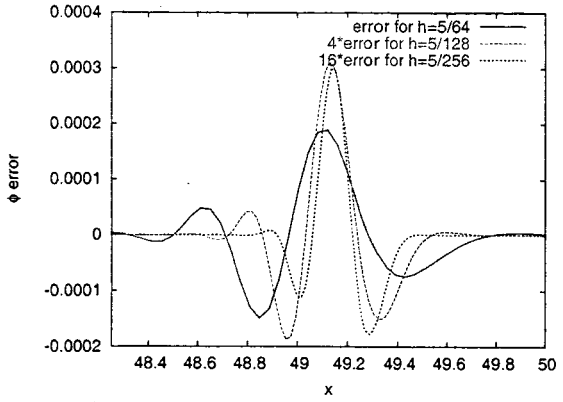

FIG. 2: Convergence plot for the error in φ. There is a refinement boundary at $x = 50$. The coarse grid spacing h of each simulation is indicated in the figure, and the medium and high resolution curves have been multiplied by 4 and 16 respectively, as appropriate to demonstrate 2nd order convergence.

To test if this model problem is sufficient, we have numerically evolved Eq. (14) using a 1-D finite difference code with a resolutions $dx = h$ for $x < x_0$ and $dx = 2h$ for $x > x_0$, realizing a refinement boundary at $x = x_0$. We evolved over the domain $0 < x < 100$ with periodic boundary conditions, using three-point upwind finite difference stencil and a mesh refinement scheme similar to that in our numerical simulations with PARAMESH. Blah Blah figure Blah Blah. ... not strongly affected by variations in the time-integration method or by changing amoung mesh-refinement interfacing schemes which are consistent with the overall second-order finite differencing accuracy.

IV. A FINITE DIFFERENCE ANALYSIS

In this section we attempt to understand the numerical behavior of the Bumpy problem Eq. (14) by constructing here an analytic model for the numerical error in our simulations. Noting that the time discretization, and the details of the interpolation scheme used in applying refinement conditions seem not to be directly linked to the problematic error features we see, we model the error with as few assumptions as possible about these details. We treat the numerical errors continuously in time, and we consider the effects of spatial finite differencing in terms of a continuous field $\varphi(x,t,h)$ representing the numerical solution at (fine-grid) resolution $dx = h$. We then expand φ in orders of h,

$$\varphi(x,t,h) = \varphi_e(x,t) + h^2 \varphi_2(x,t) + \mathcal{O}(h^3), \qquad (16)$$

Where $\varphi_e(x,t)$ is understood to be the exact solution Eq. (15). We consider the effect of our finite differencing

scheme by replacing the spatial deriative appearing in Eq. (14) with a suitable finite difference operator $\tilde{D}_h$. Thus,

$$\frac{\partial\varphi}{\partial t}(x,t,h) = \beta\tilde{D}_h\varphi(x,t,h) + f(x,t). \qquad (17)$$

As above, we include a refinement jump in the grid at $x = x_0$, represented here by applying a coarser version of the finite difference stencil in the $x > x_0$ part of the spatial domain. This will be consistent with any refinement interface algorithm which applies the same finite difference stencil in both the coarse and fine regions, and applies a interpolative guard-cell filling alrogithm at the interfaces which leads to finite differences at the interface which are consistently second-order accurate. On a uniform grid the second-order error term of a finite first derivative is generally proportional to the third derivative of the field,

$$D_h\varphi(x,t,h) = \partial_x\varphi(x,t,h) + e_2h^2\partial_x^3\varphi(x,t,h) + \mathcal{O}(h^3).$$

For the specific upwind differencing operator used in Section III, the stencil of which is,

$$D_h = \frac{1}{h}\left(-\frac{3}{2} + 2E_h - \frac{1}{2}E_{2h}\right) \qquad (18)$$

where E is the spatial translation operator defined such that $E_hf(x) = f(x+h)$, the constant error coefficient turns out to be $e_2 = -1/3$. Including the refinement jump, we have

$$\begin{aligned}\tilde{D}_h\varphi &= D_h\varphi + \Theta(x-x_0)(D_{2h} - D_h)\varphi \qquad (19)\\ &= \partial_x\varphi + (1+3\Theta(x-x_0))e_2h^2\partial_x^3\varphi + \mathcal{O}(h^3).\end{aligned}$$

Substituting into Eq. (17), and rearranging, yields

$$\begin{aligned}h^2\dot{\varphi}_2(x,t,h) &= [-\dot{\varphi}_e(x,t) + \beta\partial_x\varphi_e(x,t) + f(x,t)]\\ &\quad +h^2\beta\big[\partial_x\varphi_2(x,t,h) +\\ &\qquad e_2(1+3\Theta(x-x_0))\partial_x^3\varphi_e(x,t)\big]\\ &\quad +\mathcal{O}(h^3). \qquad (20)\end{aligned}$$

Then noting that the first term vanishes, and taking the limit $h \to 0$, we derive

$$\begin{aligned}\dot{\varphi}_2(x,t) &= \beta\partial_x\varphi_2(x,t) + \qquad (21)\\ &\qquad \beta e_2(1+3\Theta(x-x_0))\partial_x^3\varphi_e(x,t),\end{aligned}$$

where we have used the notation $\varphi_2(x,t) = \varphi_2(x,t,0)$. This is our model for generation and propagation of finite differencing error in the numerical model problem in Section III.

Since Eq. (21) is of the same form as Eq. (21) we can solve it the like fashion. We leave out the negligible $F(x+\beta t)$ in φ_e, substituting

$$\begin{aligned}f(x,t) &= \beta e_2(1+3\Theta(x-x_0))\partial_x^3\varphi_e(x,t)\\ &\simeq -\frac{\beta e_2}{v+\beta}(1+3\Theta(x-x_0))\partial_x^3F(x-vt)\end{aligned}$$

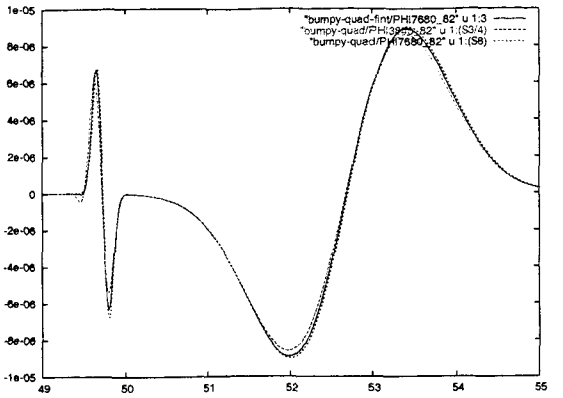

FIG. 3:

into the first line of Eq. (15). Then, performing the integral with careful attention to the presence of the step function, we get the solution

$$\begin{aligned}\varphi_2(x,t) &= (s(x-vt) - s(x+\beta t))(1+3\Theta(x-x_0))\\ &\quad +3s\Big(\frac{-v}{\beta}(x-x_0+\beta(t-\frac{x_0}{v})) \times\\ &\qquad (\Theta(x-x_0+\beta t) - \Theta(x-x_0)) \qquad (22)\end{aligned}$$

where,

$$\begin{aligned}s(x) &= \frac{\beta e_2}{(v+\beta)^2}\partial_x^2F(x)\\ &= -\frac{2\beta e_2x}{(v+\beta)^2}\exp(-x^2).\end{aligned}$$

As above, the $s(x+\beta t)$, thus the first term in Eq. (22) is effectively the differencing error associated with the upsweep in φ_e which propagates across the grid at speed v. This part grows four times larger in the coarse $x > x_0$ region. The second term is quite interesting, it propagates in the reverse direction at speed β. It has the same $s(x)$ shape as the forward propagating component, but it is reversed, and contracted by a factor β/v. It is timed to orginate at the interface as the first pulse crosses. The two terms combine make the full solution continuous at the interface. Heuristically, one could say that the second term is caused by the discontinuity in the differencing error, generated in order to produce a regular solution, and then, necessarily advecting away as required by the original model equation Eq. (14). It is contracted because it propagates at a different speed than the first term, but their time dependences must match at the interface.

V. IMPROVING THE DIFFERENCING STENCILS

The results of the last section clearly show that the reflected error in the Bumpy system is overwhelmingly due to the discontinuity in the differencing operator. More

specifically, the reflection is related to the discontinuity in the 2nd order truncation error. This observation suggests a solution.

Consider using modified differencing stencils such that the coefficient of the 2nd order truncation error in the fine grid region is multiplied by a constant factor q_0 while the coefficient of the 2nd order truncation error in the coarse grid region is multiplied by a constant factor q_1. Then the previously constant coefficient e_2 of the last section becomes:

$$e_2 \rightarrow [q_0 + (q_1 - q_0)\Theta(x - x_0)]e_2 \tag{23}$$

Repeating the steps of the last section for this new truncation error, the solution for the 2nd order error in φ becomes,

$$\begin{aligned}\varphi_2(x,t) &= (s(x-vt) - s(x+\beta t))(q_0 + (4q_1 - q_0)\Theta(x - x_0)) \\ &\quad +(4q_1 - q_0)s(\frac{-v}{\beta}(x - x_0 + \beta(t - \frac{x_0}{v})) \times \\ &\quad (\Theta(x - x_0 + \beta t) - \Theta(x - x_0))\end{aligned} \tag{24}$$

Thus for the spatially blueshifted, reflected error, we now obtain,

$$\varphi_{ref} = (4q_1 - q_0)s(-\frac{v}{\beta}(x - x_0 + \beta(t - \frac{x_0}{v}))) \tag{25}$$

Clearly, this reflected error can be eliminated simply by choosing $q_0 = q_1 = 0$. This choice corresponds to using higher order stencils, say 3rd or 4th order accurate, throughout the entire grid. However, it has been observed that higher order differencing can some times create instabilities in a strong field region (which would typically correspond to the finest grid region). So it may be useful to consider an alternative solution.

Note that with the choice $q_0 = 1$ and $q_1 = \frac{1}{4}$, the reflected error vanishes. More generally, of course, any choice of q_0 and q_1 that makes the truncation error continuous across the refinement boundary will remove the 2nd order reflection. In particular, the choice

$$q_n = \left(\frac{h_0}{h_n}\right)^2 \tag{26}$$

will work in the nth refinement region of a grid with an arbitrary number of refinement levels, where h_0 is assumed to be the grid-spacing in the finest region. We call such a scheme mesh-adapted differencing (MAD).

A 2nd order MAD stencil can be obtained simply by linearly combining a 2nd order accurate stencil with a higher order accurate stencil, as follows:

$$D_{h_n} = q_n D^{[2]}_{h_n} + (1 - q_n) D^{[j]}_{h_n} \tag{27}$$

where the superscripted numbers in square brackets represent the order of accuracy of the differencing operator, and $j > 2$. In the particular case of a 2nd order upwinded stencil combined with a 3rd order lopsided stencil, for example, the resulting stencil has the form:

$$\begin{aligned}D_{h_n} &= \frac{1}{h_n}\left[\left(-\frac{1}{3} + \frac{1}{3}q_n\right)E_{-h_n} + \left(-\frac{1}{2} - q_n\right)\right. \\ &\quad \left. + (1 + q_n)\,E_{h_n} + \left(-\frac{1}{6} - \frac{1}{3}q_n\right)E_{2h_n}\right]\end{aligned} \tag{28}$$

Implementing this MAD stencil in the Bumpy code, it is proven phenomenologically (and phrenologically) that the dominant reflected error is eliminated (Fig. 4).

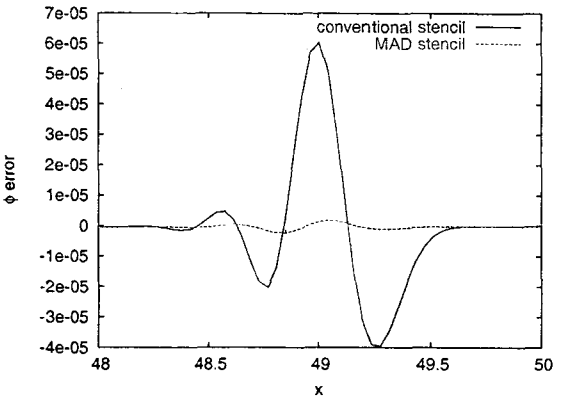

FIG. 4: Comparison of the error in φ reflected from the refinement boundary at $x = 50$ in the case of a 2nd order conventional stencil and a 2nd order MAD stencil.

VI. RESULTS FOR BLACK HOLE EVOLUTIONS

Returning to our Einstein solver, we have found that 3rd or higher order accurate differencing of advection terms is unstable in the vicinity of black hole punctures, if the stencil has any points on the "downwind" side (opposite the shift, towards the puncture). If the 3rd or higher order accurate differencing stencil does not have any points on the downwind side, it requires three or more layers of guardcells to accommodate points on the upwind side, which is expensive memory-wise. Thus, although higher order spatial differencing should reduce reflection from refinement boundaries, it is not always practical.

Use of a 2nd order accurate MAD stencil, as in Eq. (28), for advection, avoids the above difficulties. As we generally locate the punctures within the finest grid regions, and the MAD stencil automatically reverts to conventional 2nd order upwinding in this region, the advection derivative does not take any points on the downwind side in the vicinity of the puncture and we find that stability is maintained.

In this way, we have implemented a 2nd order accurate MAD stencil for advection. For all non-advection derivatives, we have implemented a linear combination of 2nd order centered and 4th order centered stencils, as in

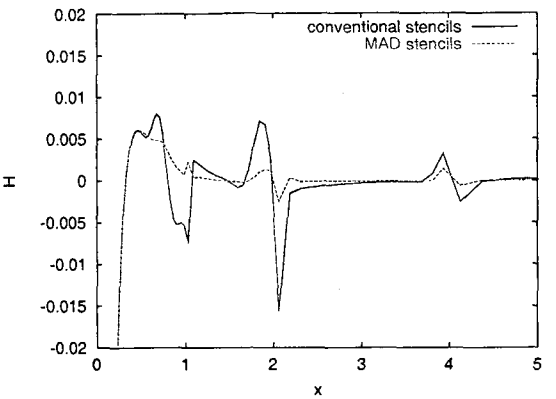

FIG. 5: Comparison of the Hamiltoniain constraint H in the case of 2nd order accurate, conventional differencing stencils and 2nd order accurate, MAD stencils. There is a single puncture black hole centered at the origin, and refinement boundaries at $|x_i| = 1M$, $2M$, and $4M$.

Eq. (27). As a result, reflection from refinement boundaries has been dramatically reduced in the case of a single puncture (Fig. 5). We have found similar improvement in the binary black hole case as well.

VII. CONCLUSIONS

We have studied a problem peculiar to advection across a mesh interface, in the form of reflections that propagate at the speed β of the advection. Effective blue-shifting of the error makes it particularly egregious. We have successfully modeled the problem analytically, and thereby found a solution. Our proposed solution, that of making the differencing error continuous across mesh interfaces, may have wide application. In addition to grids of non-uniform refinement, mesh-adapted differencing may also be appropriate for grids with multiple coordinate patches, where discontinous differencing error may also be expected.

Acknowledgments

We gratefully acknowledge CPU time grants from the Commodity Cluster Computing Project (NASA-GSFC) and Project Columbia (NASA Advanced Supercomputing Division, NASA-Ames). This work was supported in part by NASA Space Sciences grant ATP02-0043-0056. JvM was also supported in part by the Research Associateship Programs Office of the National Research Council.